CHAPTER 5

Effects of Delta-Trimethylindium-Flow-Like Process on Optical Properties of InGaN/GaN Multiple Quantum Wells

5.1 Introduction

InGaN/GaN multiple quantum wells (MQWs) are widely used as active layers in light-emitting diodes (LEDs) and laser diodes (LDs) in the ultraviolet-blue-green range [1,2]. The blue LEDs, which showed higher efficiency than that of green LEDs, have been widely used in the communication and information technologies. The Indium (In) mole fraction of 0.1-0.2 and 0.45 is required for blue and green LEDs, respectively. The phase separation or separation of In is a major problem in the InGaN system due to solid phase immiscibility between InN and GaN. At normal growth temperatures, the alloy is unstable over the entire composition. The formation of phase separation leads to a quantum dot-like structure, which is highly beneficial to obtain high external quantum efficiency from the InGaN/GaN LEDs structure [3]. In general, the trimethylindium (TMIn)-flow rate is constant during the growth of QWs. However, due to the larger lattice mismatch between InN and GaN, it is usually difficult to grow high-quality InGaN/GaN QWs to achieve good quantum confinement and high emission efficiency [4-6]. Furthermore, it also reported that the spatial In concentration fluctuations or exciton localization effects tend to control the luminescence properties in InGaN/GaN QWs with higher In concentrations in thinner wells, while quantum confined Stark effects (QCSE) dominate the recombination emission in the wide QWs [7].

In InGaN, additional contribution to band tail formation might arise from self-formed quantum dots-like regions. A number of studies have been reported using different growth processes to improve the emission efficiency of InGaN/GaN MQWs. These indicate the addition of the InN interfacial layers between the wells and barriers, trapezoid/triangular QWs, and pre-depositing of In prior to QW growth with a growth interruption between the wells and barriers [8-11]. Such processes can result in the interface improvement or the formation of QDs-like clusters for strongly localizing carriers and thus improving emission efficiency.

5.2 Experiments

All LED samples used in this study were grown on c-plane (0001) sapphire (Al_2O_3) substrates by metalorganic vapor phase epitaxy (MOVPE). The precursors of Ga, In, N, Mg and Si were TMGa, TMIn, NH_3, Cp_2Mg and SiH_4, respectively. Prior to the deposition of

GaN nucleation layer, the sapphire substrates were pre-baked at 1100°C with H_2 ambient for 10 min. The LED structures consisted of a 30-nm-thick GaN nucleation layer grown at 550°C, a 4-μm-thick Si-doped GaN layer grown at 1060°C, a 8-pair $In_xGa_{1-x}N$/GaN MQW active layers grown at 770°C, a 50-nm-thick Mg-doped AlGaN electron blocking layer grown at 1050°C, and a 0.15-μm-thick Mg-doped GaN cladding layer grown at 1050°C. For the 8-pair $In_xGa_{1-x}N$/GaN MQW active region, each pair consists of a 2.5-nm-thick $In_xGa_{1-x}N$ well layer and a 13-nm-thick GaN barrier layer. For comparison, two LED samples were grown with different initial TMIn-flow rate (f_{TMIn}) in the well layers. For sample A, the f_{TMIn} was fixed at 230 sccm for overall growth of an InGaN layer. For sample B, a δ-TMIn-flow process was used. In this process, the initial f_{TMIn} in each InGaN layer was 400 sccm persisting for a 10% growth time of an InGaN layer, and was then switched to 230 sccm. Schematic of f_{TMIn} variations during growth for samples A and B are shown in Fig. 5.1.

To analyze the microstructures of the $In_xGa_{1-x}N$/GaN MQWs, cross-sectional high-resolution transmission electron microscopy (HRTEM) measurements were performed using a Philips 420 microscope operating at 200 kV. Structural parameters, including the thickness of the well and the barrier and the In composition of *x*, were measured by high-resolution x-ray diffraction (HRXRD) using a Bede D1 triple-axis diffractometer with a parabolic graded multiplayer Gutman mirror collimator, followed by a fourbounce channel-cut Si (220) monochromator, delivering a *Cukα1* line of wavelength λ = 0.154054 nm. The asymmetric two-bounce Si (220) analyzer crystal was placed in front of the detector. Photoluminescence (PL) spectra were measured as a function of temperature ranging from 10 to 300K using the 325 nm line of a 28 mW He-Cd continuous wave laser. The fabrication of the LEDs was described in detail elsewhere [12]. The light output power was measured using a calibrated power meter with a large Si detector (detector area 10×10 mm^2) approximate 5 mm above the device.

Figure 5.2 shows (0004) reflection HRXRD θ-2θ spectra obtained from the samples A and B. The θ-2θ diffraction patterns were simulated using a computer program based on dynamical theory. The strongest peak in each spectrum originates from the GaN epilayers. The satellite (SL) peaks are marked as SL-0, SL-1 etc. for the zero order, first order diffraction peaks. Additionally, both spectra show higher order diffraction peaks, which indicates the good layer periodicity and the structural quality. Additionally, the satellite peaks in the HRXRD spectra of sample B are very obvious and clear, which implies the interface between well and barrier layers is abrupt as well as sample A. The average indium

composition of x in the well layer and the period D (well and barrier) can be determined from the relative positions of the 0*th*- and higher-order peaks in the HRXRD spectra based on the following expression [13]:

$$D = \frac{n\lambda}{2}(\sin\theta_n - \sin\theta_{0th}) \qquad \text{Eq. (5.1)}$$

where n is the order of the satellite peaks, λ is the wavelength of x-ray radiation, θ_n is their diffraction angle, and θ_{0th} is the angle of the 0*th*-order peak. According to the best fit to the measured spectra, the In concentration of x and D for both samples are similar, which are about 0.2 and 14.7 nm, respectively. As shown in table 5.1, for both sample, the FWHM of the higher-order SL peaks broaden and the FWHM of the sample B with delta-TMIn flow rate process is larger than sample A. This broadening may be caused by spatial variation of alloy composition fluctuation. Figure 5.3 shows cross-sectional HRTEM images of the MQW structure for samples A and B. The well and the barrier thickness of both samples are estimated about 2.3 nm and 12.8 nm, respectively, which is in good agreement with the structural design. In general, the dark contrast regions indicate QD-like or In-rich regions, which could be considered as the origin of the emission in the well layer [14].

Figure 5.4 shows the 10K PL spectrum of sample A and sample B which has the typical InGaN-related emission band with peak emission around 2.79 and 2.81 eV for samples A and B with a full linewidth at half-maximum (FWHM) of about 80 and 53 meV, respectively. It can be seen that the PL peak position of sample B blue shifts toward higher photon energy side while its FWHM of PL peak is smaller than that of sample A. According to reference 7, the In concentration in InGaN QWs is assumed to fluctuate spatially, thus forming deep cusps or QDs-like regions in the energy gap. This kind of QW will not have a smooth, sloping band structure that is necessary for the QCSE. The QCSE causes the separation of the electron and hole wave functions and reduce the emission intensity. The carriers will reside in localized states created by the fluctuations or QDs-like regions instead of separating to opposite sides of the well. Thus, the QCSE will be reduced or even eliminated in wells with large indium fluctuations or QDs-like regions [7]. Moreover, the confinement provided by the regions mentioned above, which effectively forms QDs, can overcome the negative effect of the polarization field [15]. As a result, a PL blue shift observed from sample B with a narrower linewidth might be due to the increase in indium fluctuations or QDs-like regions. Exciton pairs are confined in the local minima, and the cusps or QDs-like regions operate as excellent radiative recombination centers. Previous reports also indicate the InGaN/GaN MQWs with

QDs-like regions in the well layers showed high emission efficiency [8,9].

5.3 Temperature-dependent photoluminescence measurement

It is usually believed that the carrier localization mechanism is the key to the efficient photon emission in such a compound of relatively higher defect density (~10^8 cm^{-3}). Typically, the process of aggregation and hence the effect of carrier localization become stronger with increasing average content. With the effect of localization, it has been widely observed that PL spectral peak showed an S-shape variation with temperature. This temperature-dependence behavior originates from the localization of thermalized carriers and hence a blue-shift of PL spectral peak in a certain temperature range.

The PL spectra of samples A and B as a function of temperature in the range from 10 to 300K are plotted in Fig. 5.5. Both PL line-widths remain symmetric only up to 190K, and above this temperature it becomes inhomogeneously broadened. In general, band gap energies of semiconductors decrease with increasing temperature following the Varshni empirical equation [16]

$$Eg(T) = E(0) - \frac{\alpha T^2}{\beta + T} \qquad \text{Eq. (5.2)}$$

where T is temperature in Kelvin, $E(0)$ is the band gap at 0K, and α and β are known as Varshni's fitting parameters. In an alloy, the emission line is redshifted with respect to the Varshni equation. However, anomalous temperature dependence has been observed in InGaN active layers, where luminescence peak energies make a blue shift with respect to the values predicted by the Varshni's formula. Eliseev *et al.* [16] reported that such blue shifting behavior can be interpreted by the effect of localized tail states assuming that the density of state (DOS) of excitons induced by potential fluctuation. This leads to a statistical distribution of excitionic transition energies, which are assumed to have a Gaussian distribution with a standard deviation σ. The dependence of σ on composition, x, is described by [17],

$$\sigma = \gamma \frac{dE_g(x)}{dx} \sqrt{x(1-x)\frac{V_c(x)}{a^3{}_{ex}(x)\frac{4\pi}{3}}} \qquad \text{Eq. (5.3)}$$

where γ is a factor smaller than one, accounting for the quantum mechanical averaging of the excitonic wave function. $V_c(x)$ is the smallest volume in which a chane in composition may occur and a_{ex} (x) is the exciton Bohr radius. When $V_c(x)$ is the volume of the primitive unit cell, E_g presents the ultimate lower limit for σ in a perfect random alloy. Christen *et al.* [18] have shown that the redshift of the luminescence peak position due to statistical alloy

broadening in σ^2/k_BT. By introducing this term into Eg, the temperature-dependent emission energy could be fitted based on the band tail model suggested by Eliseev *et al.* as follow [19]

$$E(T) = E(0) - \frac{\alpha T^2}{T+\beta} - \frac{\sigma^2}{k_B T} \qquad \text{Eq. (5.4)}$$

the first term describes the energy gap at zero temperature in Kelvin; α and β are known as Varshni's fitting parameters. The third term comes from the localization effect, in which σ indicates the degree of localization effect. K_B is Bolzmann's constant. For study in detail, the dominated emission peaks in the PL spectra of sample A and B are shown in Fig. 5.6. It can be seen that both curves do not follow the Varshni law and shows an "S" shape (redshift-blueshift-redshift) over a temperature range from 10 to 300K, indicating clearly the existence of localized states in both samples [17-19]. The value of σ was estimated to be 14.7 and 17.9 meV for samples A and B, respectively; indicating the localization effect of sample B is stronger than that of sample A.

Generally, the internal quantum efficiency can be evaluated by the temperature dependence of the integrated PL intensity [20,21]. Fig. 5.7 show an Arrhenius plot of the normalized integrated PL intensity for the InGaN-related PL emission over the temperature range under investigation. The analysis of these data has been carried out using well-known thermal activation relation [22]

$$I(T) = \frac{I_0}{1 + C\exp(-\frac{E_a}{k_B T})} \qquad \text{Eq. (5.5)}$$

where C the constant, Ea the activation energy, and k_B the Bolzmann's constant. At T > 80 K, the integrated PL intensity is thermally activated with activation energy of about 35.3 meV and 42.8 meV, respectively, to samples A and B. For T > 80K, the thermal quenching can be fitted with activation energies E_A of 35.3 meV and 42.8 meV, respectively, to samples A and B. It has been suggested that the measured activation energy E_a in InGaN samples represents the localization energies of excitons, resulting from band edge fluctuations [23]. Generally, the quenching of the luminescence with temperature can be explained by thermal emission of the carriers out of a confining potential with an activation energy correlated with the depth of the confining potential [24]. It was inferred from the results mentioned above that the In fluctuations or the QD-like regions might be more abundant in sample B than in usual QWs (sample A). These results suggest that the composition fluctuations or QDs-like regions formed by using δ-TMIn-flow process can provide the necessary confinement for an improved recombination rate.

5.4 Photoluminescence excitation and light output performance

Photoluminescence excitation (PLE) can provide the information of absorption spectrum and understand the distribution of energy state. Fig. 5.8 shows the PL and PLE spectra of the InGaN/GaN MQWs of sample A and B at 10K. The detection energy of the PLE measurement is set at the main InGaN-related PL peak energy of sample A and B. In order to analyze the Stokes' shift, which is defined as the difference in energy between the effective band gap and the emission peak energy, it is essential to have an accurate description of the absorption edge that includes the effects of broadening. A PLE measurement was performed to get the absorption edge, Martin *et al.* suggested that by fitting the PLE spectra to the sigmoidal formula

$$\alpha = \frac{\alpha_0}{1+\exp(\frac{E_{eff}-E}{\Delta E})} \qquad \text{Eq. (5.6)}$$

where α_0 is the constant, E_{eff} is the effective band gap, ΔE the broadening parameter which indicates a distribution of absorption states , and E the excitation energy at which the intensity of emission.

A large Stokes' shift of PL peak with respect to PLE absorption peak was observed in sample A and B, which is 186 meV and 225 meV, respectively. The Stokes' shift was often attributed to carrier localization in disordered systems, such as InGaAs/GaAs QDs or InGaN/GaN MQW structures. And ΔE is the broadening parameter representing the degree of composition fluctuation. The larger value indicates the large inhomogenous. The ΔE is 65 meV and 66 meV for sample A and sample B, respectively. The localization within the dots leads to the Stokes' shift. The increase in absorption edge broadening as the emission peak energy decreases is the result of greater tailing of the JDOS for layers containing increasingly large dots, caused by fluctuations resulting form variation in dot size or shape.

The fabricated LED samples were tested for their light outputs as a function of injection current (L-I) as shown in Fig. 5.9. As can see the emission power intensity of sample B is higher than that of sample A for overall driving-current range. At lower driving current of 20 mA, the sample B have a light output power of ~ 3.6 mW 16% greater than ~ 3.1 mW for the sample A. The enhancement of light output increases with the driving current up to ~24% at 60 mA.

In summary, the effects of δ-TMIn-flow process with an initial f_{TMIn} of 400 sccm during the well layer growth on the optical properties of InGaN/GaN MQWs were investigated. The results show that the δ-TMIn-flow process can improve the localization effects and the

activation energy. The light output of the GaN LEDs with the δ-TMIn-flow process is increased up to 24% without obvious deterioration of interfacial abruptness.

Table 5.1 Summary of the x-ray result for sample A and B.

FWHM (arcsec)	**SL-1**	**SL-2**	**SL-3**
Sample A	364	382	400
Sample B	400	472	688

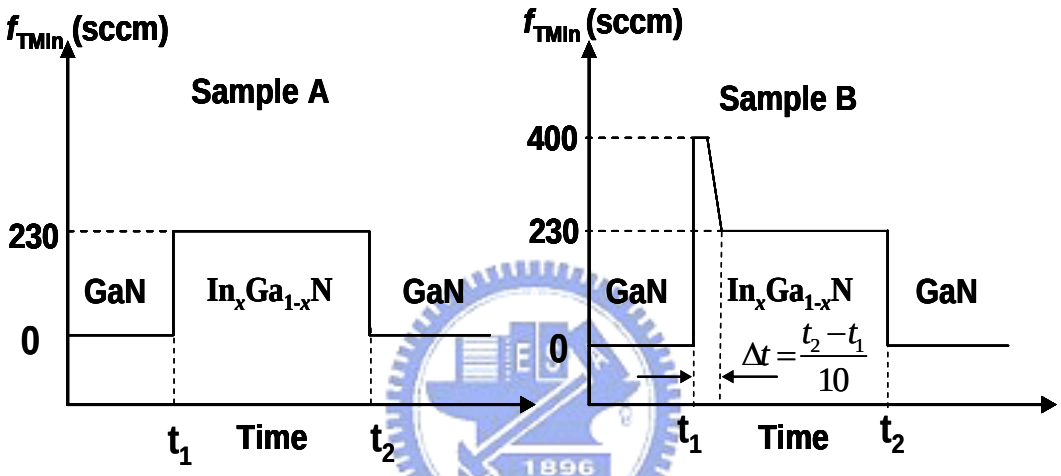

Fig. 5.1. Schematic diagrams of fTMIn variation over time in InGaN QWs for samples A and B.

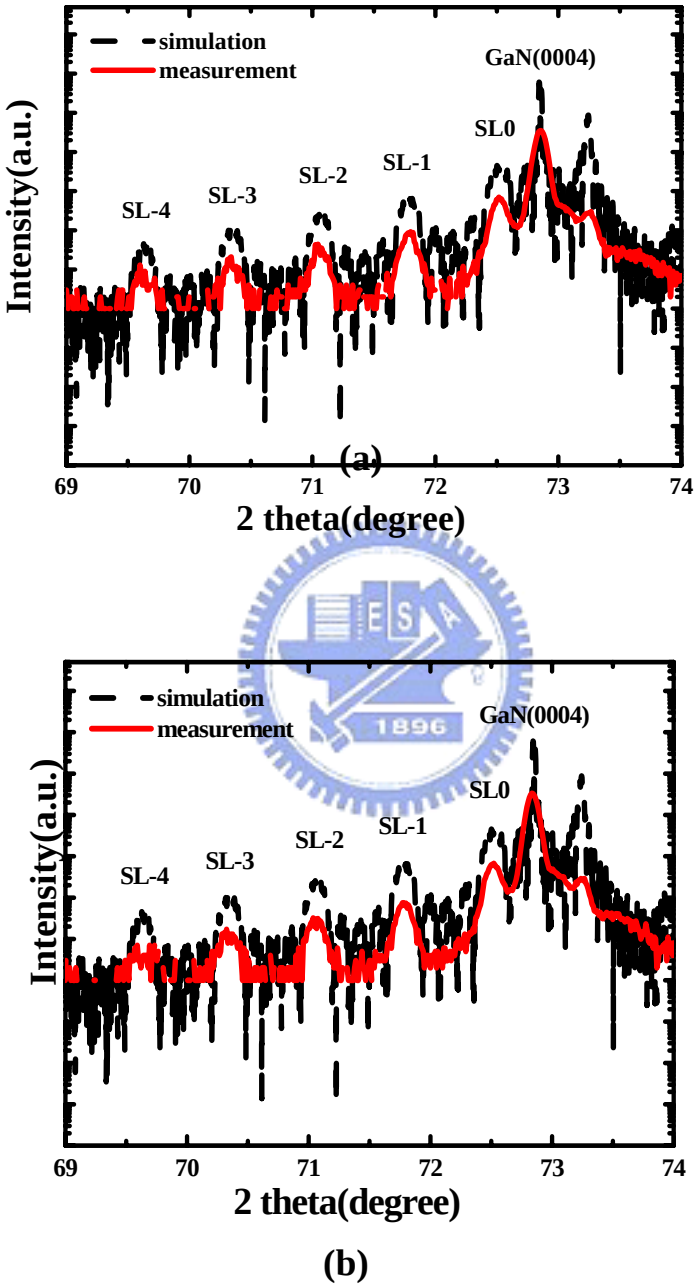

Fig. 5.2. HRXRD spectra for (0004) reflection from the InGaN/GaN MQW structure of (a) sample A, (b) sample B.

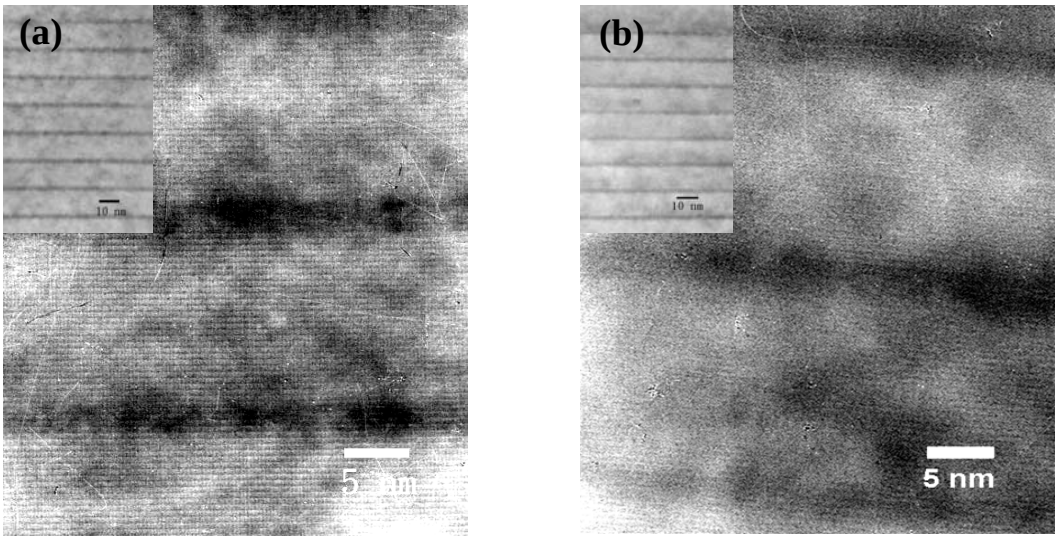

Fig. 5.3. Cross-sectional TEM image of the InGaN/GaN MQWs of (a) sample A, (b) sample B. The insets in (a) and (b) are the enlarged view of the whole MQWs structure.

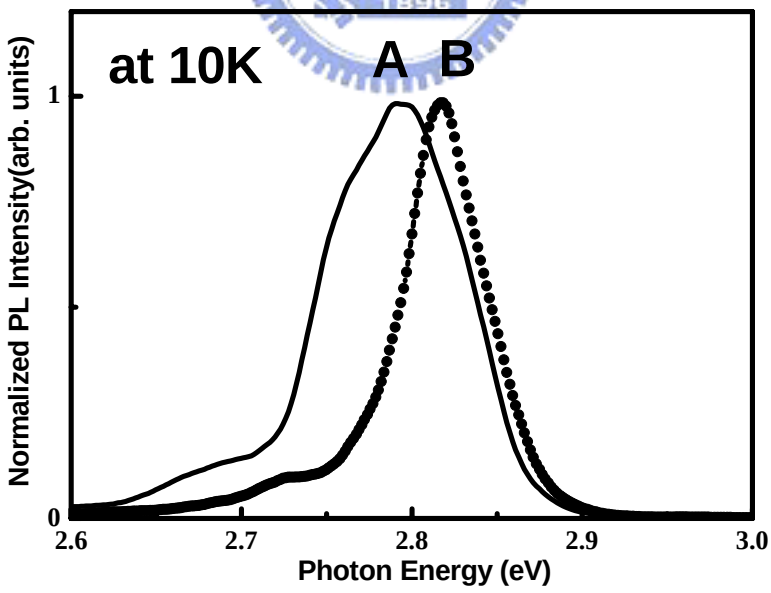

Fig. 5.4. The normalized PL emission spectra of samples A (solid line) and B (solid circle) at 10K.

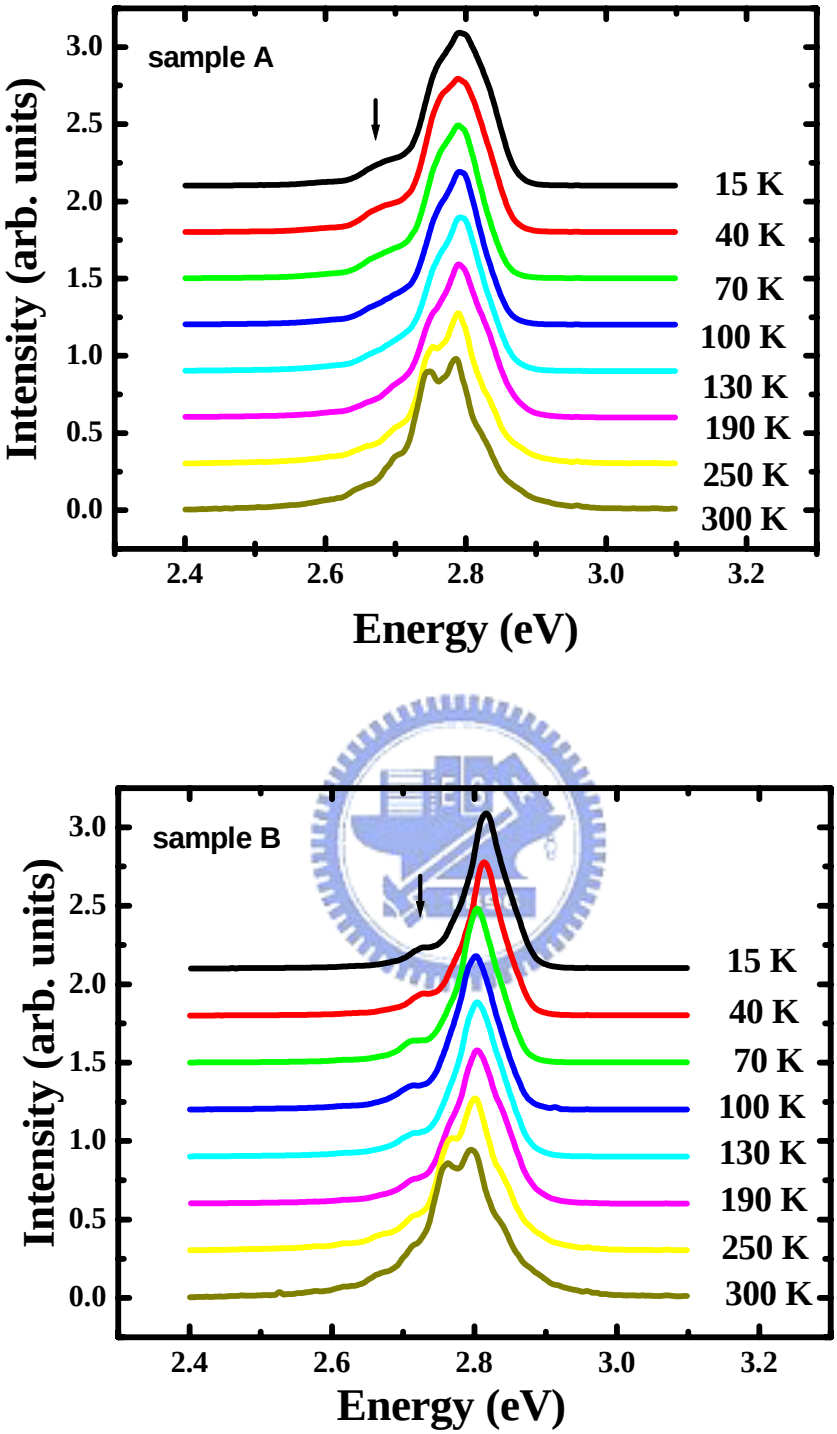

Fig. 5.5. Temperature-dependent PL spectra of sample A (left) and B (light).

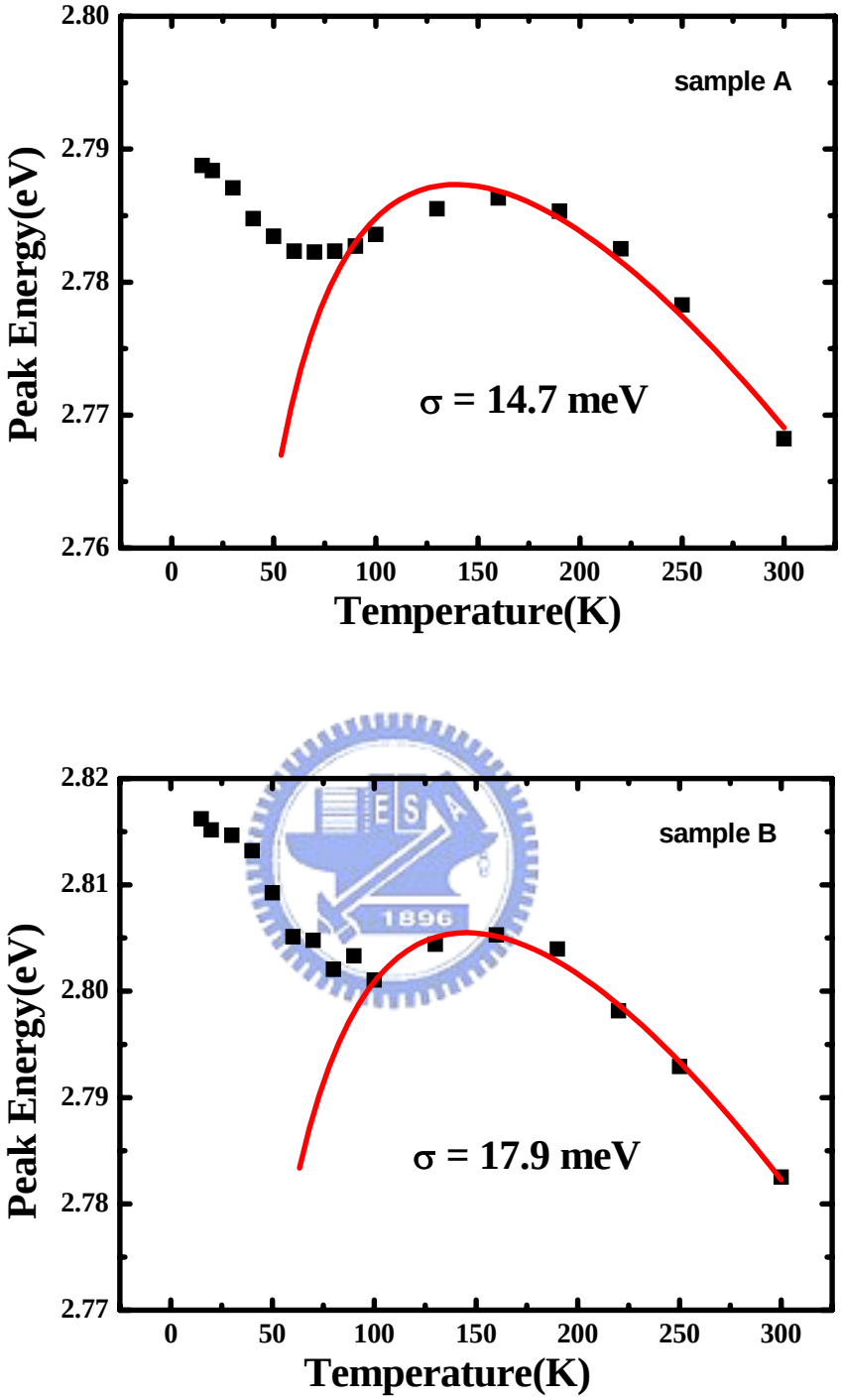

Fig. 5.6. Arrhenius plots of the normalized integrated PL intensity for the InGaN-related PL emission of sample A and B over the temperature range under investigation.

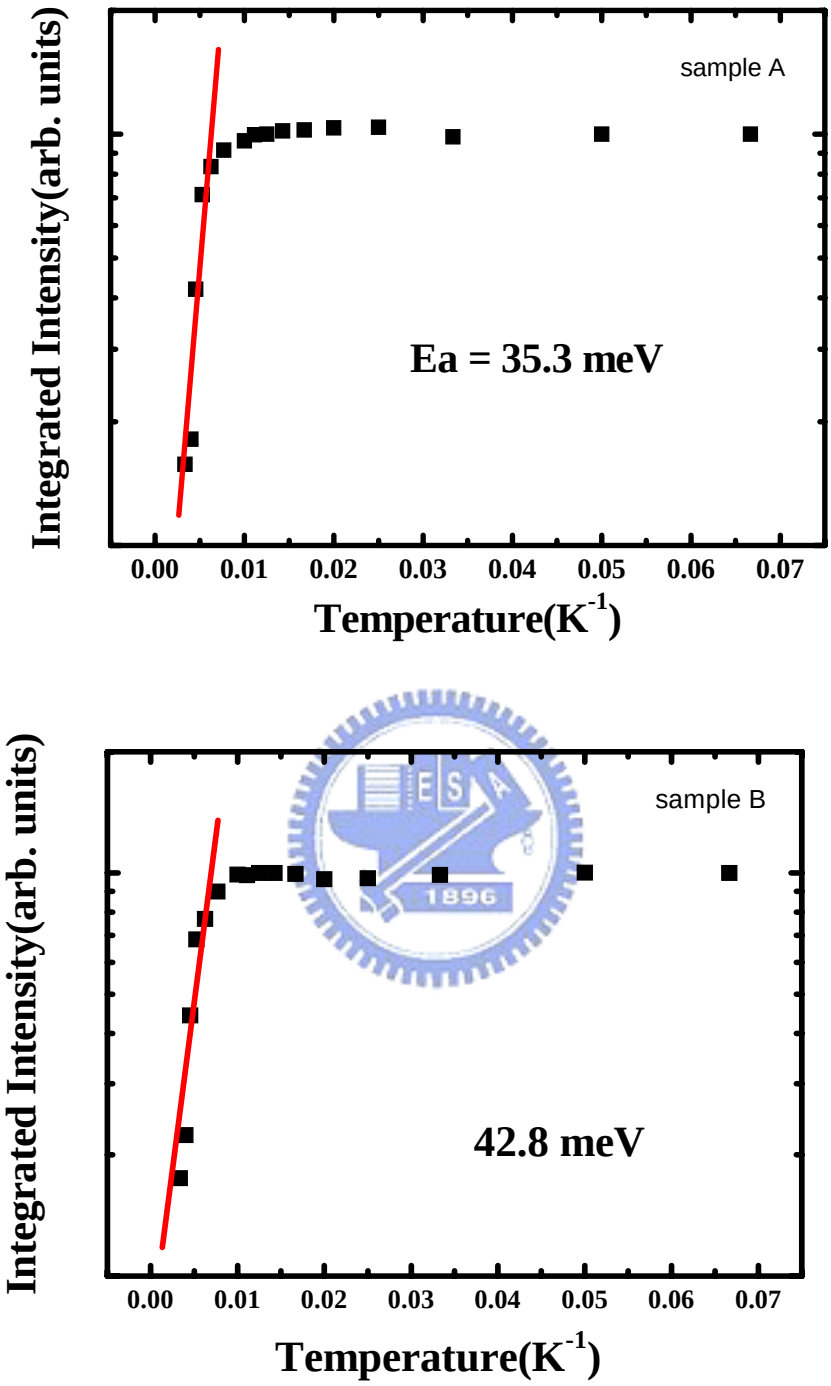

Fig. 5.7. The normalized PL intensity as a function of T^{-1} for sample A and B.

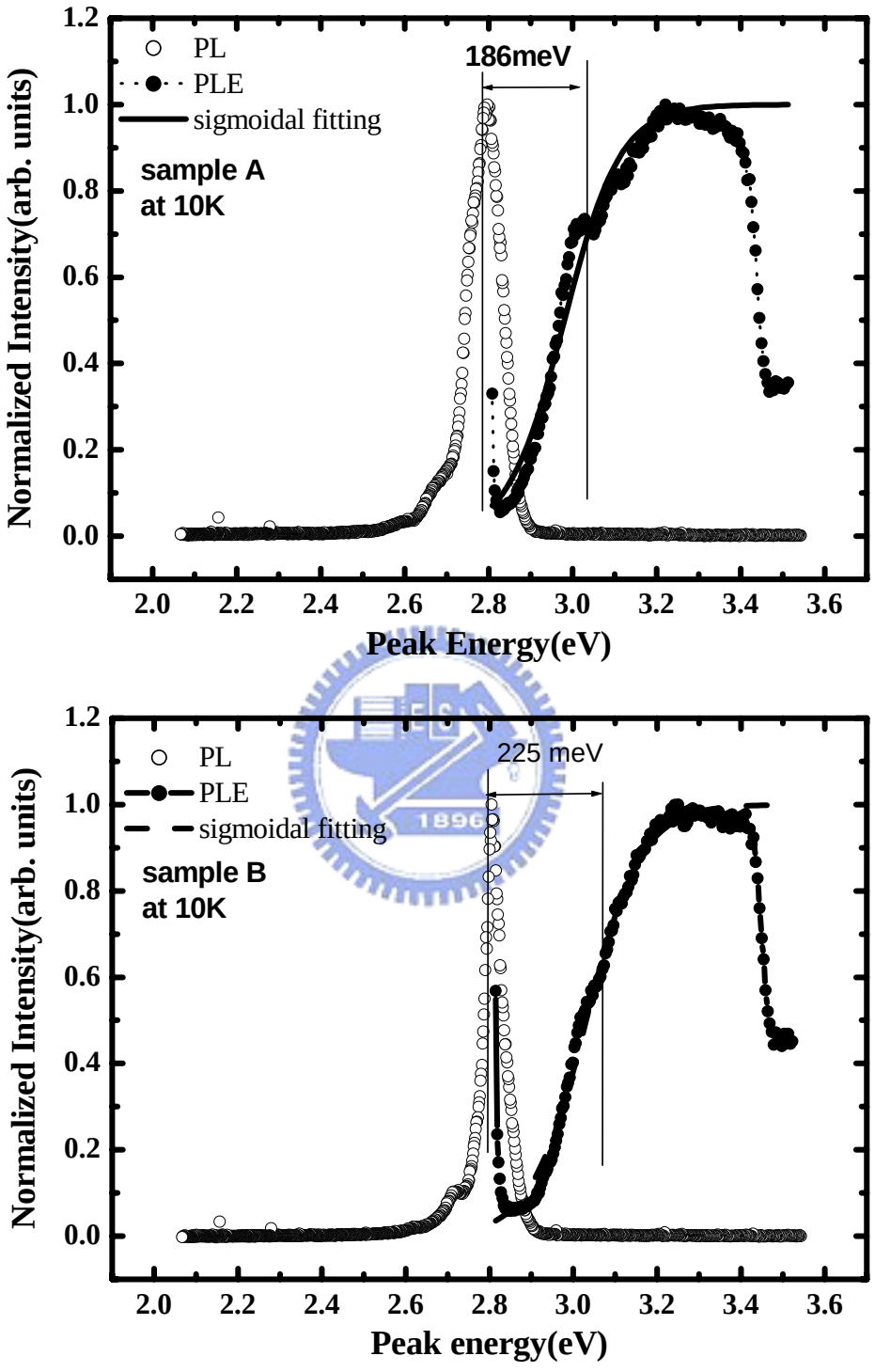

Fig. 5.8. PL and PLE spectra of the InGaN/GaN MQWs of sample A and B at 10K.

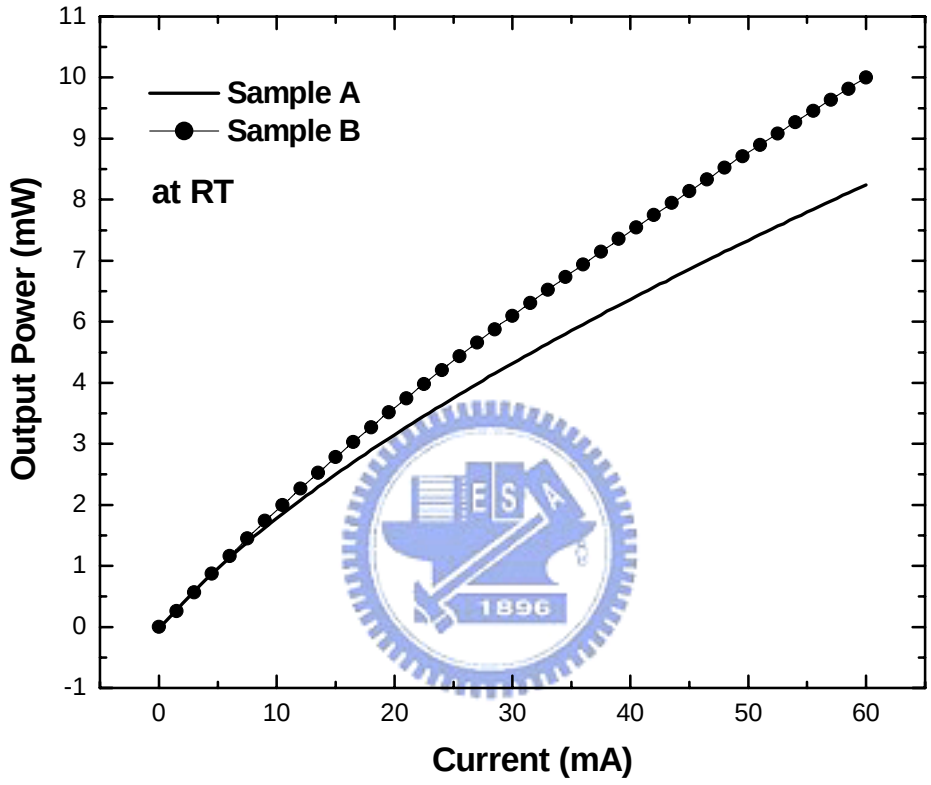

Fig. 5.9. *L-I* characteristics for the LEDs of samples A and B.

Reference

[1] S. Nakamura and S. F. Chichibu, Introduction to Nitride Semiconductor Blue Lasers and Light Emitting Diodes (Taylor & Francis, New York, 2000).
[2] Y. Narukawa, Y. Kawakami, M. Funato, S. Fujita, and S. Nakamura, Appl. Phys. Lett. 70, 981 (1997).
[3] N. Grandjean, B. Damilano, J. Massies, and S. Dalmasso, Solid State Commun. 113, 495 (2000).
[4] K. Watanabe, J. R. Yang, N. Nakanishi, K. Inoke, and M. Shiojiri, Appl. Phys. Lett. 80, 761 (2002).
[5] H. K. Cho, J. Y. Lee, N. Sharma, C. J. Humphreys, G. M. Yang, C. S. Kim, J. H. Song, and P. W. Yu, Appl. Phys. Lett. 81, 3102 (2002).
[6] Y. S. Lin, K. J. Ma, C. Hsu, S. W. Feng, Y. C. Cheng, C. C. Liao, C. C. Yang, C. C. Chuo, C. M. Lee, and J. I. Chyi, Appl. Phys. Lett. 77, 2988 (2000).
[7] N. A. Shapiro, P. Perlin, C. Kisielowski, L. S. Mattos, J. W. Yang, and E. R. Weber, MRS Internet J. Nitride Semicond. Res. 5, 1 (2000).
[8] Y. C. Cheng, C. M. Wu, M. K. Chen, C. C. Yang, Z. C. Feng, G. A. Li, J. R. Yang, A. Rosenauer, and K. J. Ma, Appl. Phys. Lett. 84, 5422 (2004).
[9] M. G. Cheong, C. Liu, H. W. Choi, B. K. Lee, E. –K. Suh, and H. J. Lee, J. Appl. Phys. 93, 4691 (2003).
[10] R. J. Choi, H. W. Shim, S. M. Jeong, H. S. Yoon, E. –K. Suh, C. –H. Hong, H. J. Kee, and Y. –W. Kim, Phys. Stat. Sol. (a) 192, 430 (2002).
[11] J. P. Liu, R. Q. Jin, J. J. Zhu, J. C. Zhang, J. F. Wang, M. Wu, J. Chen, Y. T. Wang, and H. Yang, J. Crystal Growth 264, 53 (2004).
[12] J. K. Sheu, C. H. Kuo, S. J. Chang, Y. K. Su, L. W. Wu, Y. C. Lin, J. M. Tsai, R. K. Wu, and G. C. Chi, IEEE Photonics Technology Letters 15, 18 (2003).
[13] I. H. Kim, H. S. Park, Y. I. Park, and T. Kim, Appl. Phys. Lett. 73, 1634 (1998).
[14] S. Nskamura, M. Senoh, S. Nagahama, N. Iwasa, T. Yamada, T. Matsushita, Y. Sugaimoto, and H. Kikyokau, Appl. Phus. Lett. 70, 2753 (1997).
[15] M. B. Nardelli, K. Rapcewicz, and J. Bernholc, Appl. Phys. Lett. 71, 3135 (1997).
[16] Y. P. Varshni, Physica **34**, 149 (1967).
[17] A. Bell, S. Srinivasan, C. Plumlee, H. Omiya, F. A. Ponce, J. Christen, S. Tanaka, A. Fujioka, and Y. Nakagawa, J. Appl. Phys. 95, 4670 (2004)
[18] J. Christen, and D. Bimberg, Phys. Rev. B 42, 7213 (1990).
[19] P. G. Elixeev, P. Perlin, J. Lee, and M. Osinski, Appl. Phys. Lett. 71, 569 (1997).
[20] T. Wang, P. J. Parbrook, W. H. Fan and A. M. Fox, Appl. Phys. Lett. 84, 5159 (2004).
[21] H. Q. Ni, Z. C. Niu, X. H. Xu, Y. Q. Xu, W. Zhang, X. Wei, L. F. Bian, Z. H. He, Q. Han and R. H. Wu, Appl. Phys. Lett. 84, 5100 (2004).
[22] D. Bimberg, M. Sondergeld, and E. Grobe, Phys. Rev. B 4, 3451 (1971).
[23] M. Smith, G. D. Chen, J. Y. Lin, H. X. Jiang, M. Asif Khan, and Q. Chen, Appl. Phys. Lett. **69**, 2837 (1996).
[24] Y. H. Cho, G. H. Gainer, A. J. Fischer, J. J. Song, S. Keller, U. K. Mishra, and S. P. DenBaars, Appl. Phys. Lett. 73, 1370 (1998).